FORECASTING STORM-SNOW AVALANCHES USING A COMBINED SHEAR AND ANTICRACK INSTABILITY MATRIX
INTERNATIONAL SNOW SCIENCE WORKSHOP 2026, WHISTLER, CANADA

Benjamin H. Silberman[1*], Eric R. Pardyjak[1], Dhiraj K. Singh[1], Jim Steenburgh[1] Steven Clark[2], Travis Morrison[1,3], Jack Eskeland[3]

1 University of Utah, Salt Lake City, UT, USA
2 Utah Department of Transportation
3 Utah Avalanche Center
** Indicates the presenting author*

ABSTRACT: Forecasting storm-snow avalanches remain challenging due to limited access to the mechanical properties of snow during active snowfall and the lack of a unified framework that captures multiple failure modes. This work presents a physics-based avalanche decision-support system that combines a shear-strength stability index (SI_{sh}) with an anticrack stability index (SI_{ant}) to generate a more comprehensive stability matrix. This stability matrix is designed to provide a practical tool for identifying unstable storm-snow conditions and distinguishing between shear-driven and anticrack-driven failure mechanisms. The proposed framework leverages real-time measurements from a Differential Emissivity Imaging Disdrometer (DEID) to capture snow microstructure and density, which are used to drive both stability indices. These indices are combined into a two-dimensional decision matrix that enables intuitive interpretation of snowpack stability for avalanche practitioners. To extend beyond nowcasting, the stability matrix is coupled with output from the High-Resolution Rapid Refresh (HRRR) weather model, allowing forecasts of storm-snow instability up to 48 hours in advance. Model performance will be evaluated using georadar detections, infrasound records, and manual avalanche observations within Little Cottonwood Canyon, Utah. These datasets will be combined with additional storm-specific information such as precipitation intensity and detailed Utah Department of Transportation (UDOT) mitigation records, to inform how these avalanches failed, and on what layer of snow. Preliminary results of model validation with georadar and infrasound avalanche detection systems will be presented. Additional results will include comparisons with avalanche observations submitted to the Utah Avalanche Center. These model comparisons will be visualized through clear, informative graphics for easy interpretation by snow operationalists.

KEYWORDS: avalanche forecasting, storm-snow, anticrack, shear strength, stability index, densification

1. INTRODUCTION

Predicting when and where storm-snow (snow that has fallen within the prior 12 hours) will fracture and potentially release large-scale avalanches is of utmost importance for ensuring safe travel along avalanche-affected highways. Forecasting storm-snow avalanches remains difficult because weather hazards prevent practitioners from quantifying physical and mechanical properties such as snowflake crystal type, density (ρ_s), shear strength (Σ_s), and critical fracture energy (G_{I_c}). As a result, these measurements are often collected after a storm has concluded, when access is safe, or when samples are brought back to the laboratory, potentially resulting in changes in the snow properties (Chernov, 2024; Jamieson and Johnston, 2001; Kojima 1967).

The inability to capture individual snowflake properties is what, in large part, inspired the work of Singh et al. (2021; 2024) to develop the Differential Emissivity Imaging Disdrometer (DEID). The DEID uses thermal imaging to measure snowflakes on a particle-by-particle basis, providing properties such as ρ_s and snowflake area (A_s) in near-real-time during snowstorms. This led to work by Morrison et al. (2023), Silberman et al. (2026), and Eskeland (2025), who drove stability models using DEID measurements.

Morrison et al. (2023) proposed two new non-dimensional parameters: shape density index (SDI) and complexity (Cx) as physical properties of snowflakes that can be used to model snowpack mechanics that indicate stability. Silberman et al. (2026) validated this hypothesis by developing and validating a storm-snow-specific power-law model used to predict Σ_s;

* Corresponding author address:
Benjamin H. Silberman, University of Utah,
Salt Lake City, UT 84116;
tel: +1 781-234-4125
email: b.silberman@utah.edu

https://doi.org/10.15788/1790098590

$$\Sigma_s = \Sigma_0\, SDI \left(\frac{\rho_s}{\rho_i}\right)^{Cx}, \tag{1}$$

where Σ_0 is a relative shear strength value (Pa) fit to storm-snow data and $\rho_{\mathrm{i}} = 918$ kg m^{-3} is the density of ice. Similarly, Eskeland built on the work of McClung (2007) and proposed that G_{I_c}, which is the minimum energy required per unit area to propagate a crack through a buried layer of snow, may be modeled as

$$G_{I_c} = Cx \left(\frac{\rho_s}{\rho_i}\right)^{2Cx}, \tag{2}$$

where Cx is the average complexity of the buried layer.

Σ_s and G_{I_c} are critical in driving the available models used to predict snowpack stability within storm-snow. This work focuses on two of those models; the SNOw Slope Stability (SNOSS) model, which defines a stability index (SI_{sh}) as the ratio of Σ_s of buried layers to imposed shear stress from overlying snow, W (Hayes et al., 2004; Conway and Wilbour, 1999), and an anticrack-based stability index (SI_{ANT}), which defines a stability index as the ratio of G_{I_c} to the gravitational potential energy, W_g (Bair et al., 2012; Heierli and Zaiser, 2006).

At present, no single framework combines the shear-based and anticrack-based stability indices to capture storm-snow avalanche mechanics. To address this, we present a Data Enabled Now/forecast Dashboard for Real-time Instability Tracking and Evaluation tool, which we call DENDRITE, which computes and displays each of these stability indices in near real time. These indices are then combined, creating a stability matrix, which tracks the minimum SI values (representing the weakest layer of snow) along the trajectory of a given storm. To assess the accuracy of this matrix, preliminary model results from Little Cottonwood Canyon in Alta, UT are compared with avalanche observations from GeoPrevent's radar-based system, and Snowbound Solution's infrasound detection system (Johnson et al., 2018; Meier et al., 2016). The result is the framework for an operational decision-support tool that snow safety professionals can consult in real time during active storms.

2. DEVELOPING A STABILITY MATRIX

2.1 *The densification of storm-snow*

Each of the indices discussed in this paper rely on the evolution of snow density (ρ_s) with time. While the DEID measures ρ_s on a particle-by-particle basis, the stability indices rely on densified snow, which can be modeled as a function of both snowpack height (z) and time (t) (Kojima, 1967);

$$\frac{1}{\rho_s(z,t)}\frac{d\rho_s}{dt} = \frac{1}{\eta_s(z,t)}[\sigma_m(t) + \sigma_s(z,t)]. \tag{3}$$

Here, η_s is the compactive viscosity of a given layer of snow (Pa s), σ_s is the slope-normal overburden stress of accumulating snow (Pa), and $\sigma_m = 75$ Pa is a constant representing the contribution of metamorphic processes to densification.

Equation 3 indicates that η_s is a critical parameter when modeling the densification of storm-snow. Ongoing work aims to constrain η_s from DEID measurements directly; however, current data are insufficient to implement those findings here. Therefore, in this paper, we calculate η_s using the known viscous constitutive relationship for dry snow (Kojima, 1967) fit with an Arrhenius temperature term following Conway and Wilbour (1999);

$$\eta = B_1 \exp\left(\frac{E}{RT}\right) \exp\left(B_2 \frac{\rho_s}{\rho_{\mathrm{i}}}\right), \tag{4}$$

where $B_1 = 6.5 \times 10^{-7}$ Pa s, $B_2 = 19.3$, $E = 67.3$ kJ mol^{-1} is the activation energy, $R = 8.314 \times 10^{-3}$ kJ mol^{-1} K^{-1} is the universal gas constant, T is snow temperature (K), ρ_s is the current layer density kg m^{-3}, and ρ_i is the density of ice

2.2 *Shear-based stability index (SI_{sh})*

Each stability index presented in this paper is calculated using two methods: one which leverages DEID-measured snowflake properties (SDI and Cx) to capture snowflake habit (Silberman et al., 2026), and one which relies on empirically derived coefficients and requires only ρ_s. The former is physically-motivated, grounded in particle-level measurements, while the latter serves as a generalized alternative deployable without a DEID instrument. This two-method approach applies to both SI_{sh} (via Σ_s) and SI_{ANT} (via G_{I_c}), and all four variants are summarized in Table 1.

The SNOSS model quantifies snow stability as a competition between loading by new precipitation and strengthening of buried snow layers (Hayes et al., 2004; Conway and Wilbour, 1999). This drives a stability index, expressed as

$$SI_{sh}(z,t) = \frac{\Sigma_s(z,t)}{W(z,t)}, \tag{5}$$

where Σ_s is modeled using either the DEID-based or generalized method described above. W, the downslope gravitational shear load, is determined by snow accumulation expressed as snow water equivalent (R_{SWE}) and is calculated as

$$W(z,t) = g \int R_{SWE}(t) \sin\theta \cos\theta \, dt. \qquad (6)$$

The SNOSS model was developed as a simplified operational framework that can be modified using DEID measurements of precipitation, ρ_s, and temperature. Individual snow layers are tracked through time, capturing both progressive shear loading and the evolution of ρ_s and therefore Σ_s of buried layers.

Table 1: Comparison of DEID-based and empirically fitted formulation for storm-snow shear strength (Σ_s) and critical fracture energy (G_{I_c}).

Property	***DEID-measured formulation***	***DEID-measured parameters used***	***Empirically fitted formulation***
Shear strength, Σ_s	$\Sigma_s = \Sigma_0 \, SDI \left(\frac{\rho_s}{\rho_i}\right)^{Cx}$	Σ_0, SDI, Cx	$\Sigma_s = 530 \left(\frac{\rho_s}{\rho_i}\right)^{1.06}$
Critical fracture energy, G_{I_c}	$G_{I_c} = Cx \left(\frac{\rho_s}{\rho_i}\right)^{2Cx}$	Cx	$G_{I_c} = 0.071 \left(\frac{\rho_s}{\rho_i}\right)^{1.5}$

2.3 Anticrack-based stability index (SI_{ANT})

Recent studies (Bair et al., 2012; Adams et al., 2024) have investigated volumetric collapses within weak layers of the snowpack, causing mixed-mode failures to propagate and release storm-snow avalanches. This collapse, referred to as the anticrack failure, is modeled as a ratio of the critical fracture energy, G_{Ic}, of a buried snow layer, to the gravitational potential energy, W_g, of the slab sitting on top;

$$SI_{ANT}(z,t) = \frac{G_{I_c}(z,t)}{W_g}. \qquad (7)$$

G_{I_c} is likewise calculated using either the DEID-based or generalized method (Eskeland, 2025) described in section 2.2.

Work thus far has been performed after storms are completed, allowing for the identification of weak layers through methods such as propagation saw tests (Bair et al., 2012), known crystal types (Heierli and Zaizer, 2006), and tiltboards (Eskeland, 2025). By locating a weak layer of snow, the slab height (H) and the height of the weak layer (h) are found and used to calculate the slab potential energy W_g,

$$W_g = \rho_s H g h, \qquad (8)$$

where g is the gravitational acceleration.

This work is unique in that it seeks to develop a real-time avalanche decision-support tool. This implies that weak layers need to be located as a snowstorm is progressing. To handle this, we deploy a similar technique described in Section 2.2 to track individual layers of snow and treat each one as a potential weak layer. While $\mathrm{SI_{sh}}$ recalculates the stability model every 10 minutes, $\mathrm{SI_{ANT}}$ discretizes snow layers every 10 mm, rerunning the model each time 10 mm of snow accumulates. Visualizations of results using these methods are presented in Section 3.

2.4 Integrating SI_{sh} and SI_{ANT}

The stability indices presented in Sections 2.2 and 2.3 can be used to identify where weak layers within storm-snow are present. Each index captures a distinct mechanism and therefore carries independent diagnostic value. Thus, they are most useful when combined to predict storm-snow avalanches. This led to the development of a novel *stability matrix* (SNOSS-ANT), presented as Fig. 1. Here, the minimum SI value for each of the models (representing the weakest layer of snow) is traced along the trajectory of a given storm. This helps visualize when each of the stability indices signifies a stable or unstable snowpack, with the most stable snowpack resulting from SI_{sh} and $SI_{ANT} > 1$.

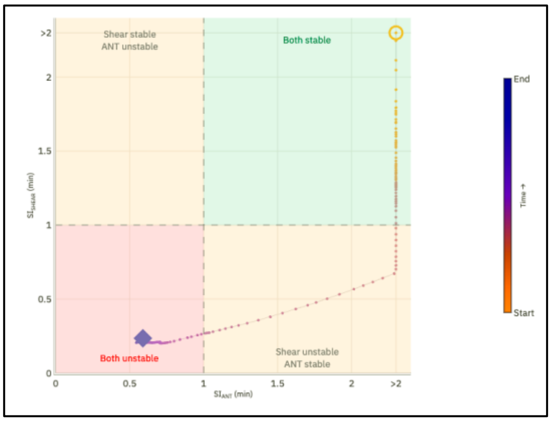

Figure 1. Combined stability matrix (SNOSS-ANT) for the January 13-15, 2024 storm. Each point represents the minimum SI_{sh} and SI_{ANT} values at a given 10-minute timestep, tracking the weakest layer of snow through time (orange = storm start, blue = storm end). The dashed lines at SI = 1 divide the matrix into four quadrants: both stable (SI_{sh} > 1, SI_{ANT} > 1; green), both unstable (SI_{sh}< 1, SI_{ANT} < 1; red), shear stable/anticrack unstable (upper left; pink), and shear unstable/anticrack stable (lower right; pink). The storm start is marked by an open circle and the end by a filled diamond.

3. DENDRITE

The stability models described in Section 2 are implemented within DENDRITE, an interactive storm-snow decision tool that integrates DEID measurements with real-time metrological and avalanche observational data to support snowpack instability assessment during active storms. The interface is organized into three panels: Stability Profiles, displaying each two-dimensional SI heatmap and the combined stability matrix; Weather Data, which compares DEID-measured precipitation accumulations and density profiles with synoptic weather observations from nearby weather stations; and Avalanche Data, summarizing timestamped observations from four independent sources (automated detection systems and user observations).

3.1 Weather data

The Weather Data panel presents four storm condition metrics compared to three separate nearby synoptic weather stations; Atwater Snow-Study Plot (ATRU1, 2682 m above sea level, same location as the DEID), the Alta Guard House (AGD, 2656 m above sea level, ~0.1 km from the DEID), and Alta-Collins Snow-Study Plot (CLN, 2945 m above sea level, ~1.5 km south of the DEID). Two time series track cumulative snow and snow water equivalent (SWE) through each storm event, with synoptic weather data for corresponding storms plotted atop DEID. A density histogram provides a compact view of the distribution of DEID-measured 10-minute bulk density across the full storm window. An additional density profile subpanel includes both the DEID-measured density and the densification-model-adjusted density against storm snow height, helping highlight snowpack structure. It is the densified profile that feeds all four SI calculations in the Stability Profiles panel.

Figure 2 shows the density profile for the January 13-15, 2024 storm in Little Cottonwood Canyon. The DEID-measured fresh density captures 10-minute averages of individual snowflake ρ_s making up the approximately 1100 mm of storm accumulation. The densification model increases density in lower layers where overburden has had more time to compact the snow, producing a profile that diverges significantly from the fresh-snow measurements. Synoptic weather stations (ATRU1 = 150 kg m^{-3}, CLN = 63 kg m^{-3}, AGD = 67 kg m^{-3}) provide single bulk density estimates for comparison, illustrating storm-dependent variability between instruments.

Figure 3 presents the weather panel for the same event. The DEID recorded approximately 1109 mm of snow accumulation, broadly consistent with the nearby AGD site (~1361 mm) and CLN (~1067 mm), and substantially higher than ATRU1 (~635 mm), reflecting again, instrument variability.

SWE accumulation reached approximately 88 mm. The density histogram shows a concentration of 10-minute bulk densities below 120 kg m^{-3}, demonstrating a low-density storm.

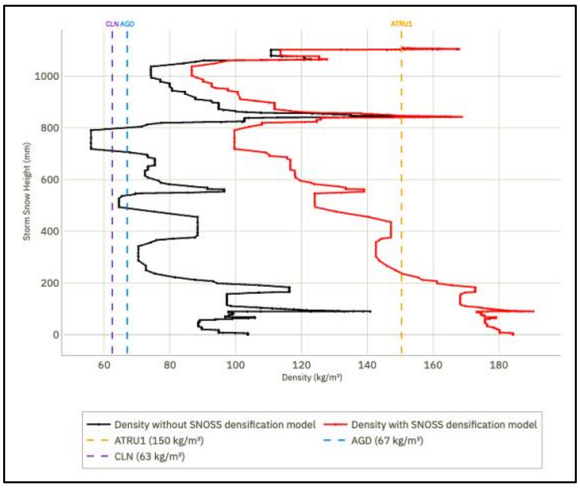

Figure 2: Density profile for the January 13-15, 2024 storm. Black: fresh DEID-measured density. Red: density after applying Eq. 3. Dashed vertical lines indicate bulk density measurements from synoptic weather stations (AGD, CLN, ATRU1).

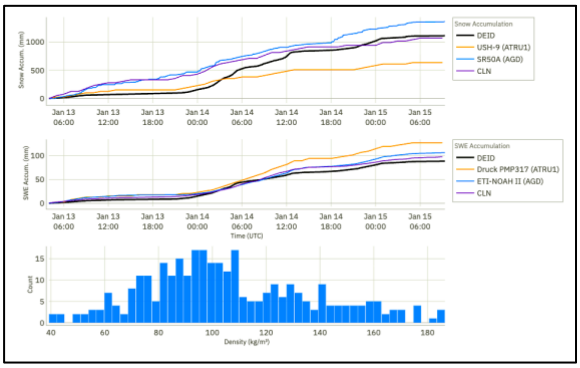

Figure 3: Weather data panel for the January 13-15, 2024 storm. Top: cumulative snow accumulation (mm) for the DEID and three synoptic stations (ATRU1, AGD, CLN). Middle: cumulative SWE accumulation (mm). Bottom: histogram of 10-minute bulk density measured by the DEID (kg m^{-3}).

3.2 Stability profiles

Both the DEID-based and best-fit formulations of SI_{sh} and SI_{ANT} (Table 1) are computed and displayed, allowing direct comparison between the physically motivated DEID-based predictions and the generalized best-fit alternatives. In each formulation, a two-dimensional heatmap is presented, tracking stability index values on a layer-by-layer basis.

Figures 4 and 5 show the DEID-based SI_{Sh} and SI_{ant} heatmaps for the January 13-15, 2024 storm. The SI_{sh} heatmap (Fig. 4) is dominated by red (SI < 1): 73% of tracked layer-time combinations are shear-unstable, with the index dropping below 1 across virtually the entire snowpack

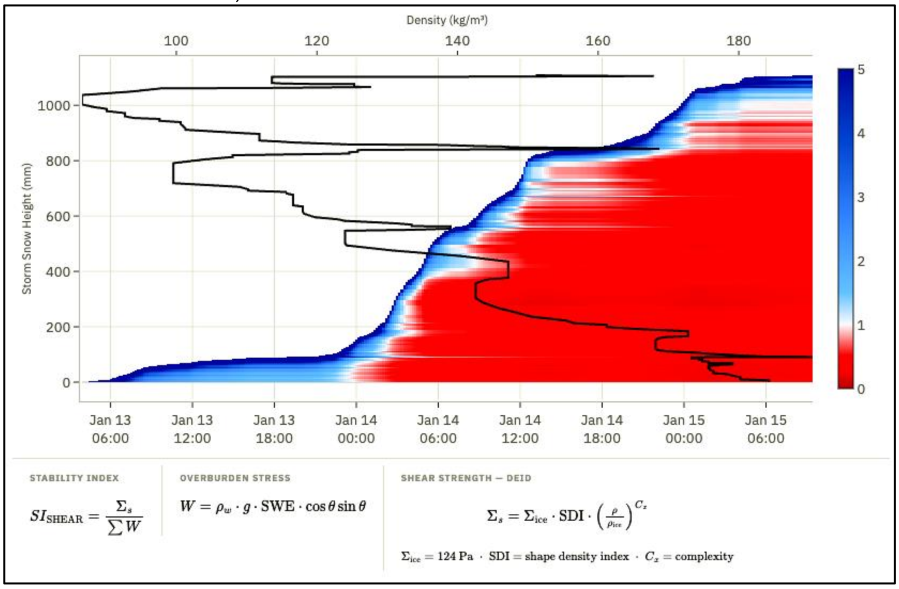

Figure 4. DEID-based shear stability index (SI_{sh}) heatmap for the January 13–15, 2024 storm. The y-axis is storm snow height (mm); the x-axis is time (UTC). Blue: $SI_{sh} > 1$ (stable); red: $SI_{sh} < 1$ (unstable). The overlaid black line shows the DEID-measured density profile after a storm ends and the snow is densified. Shear instability develops across 73% of tracked layer-time combinations.

depth by approximately 23:00 UTC on January 13 (19 hours after snow began accumulating). The physical mechanism is straightforward; fresh snowflake densities of 56–167 kg m⁻³ yield proportionally low shear strength ($\Sigma_s \propto \rho^{Cx}$), while the rapidly accumulating SWE-based overburden grows independently of density; the ratio Σ_s/W therefore falls below unity once sufficient snow has loaded the buried layers.

The SI_{ant} heatmap (Fig. 5) tells a markedly different story: 65% of layer-time combinations remain anticrack-stable (blue) throughout the storm. Unlike SI_{sh}, the anticrack index G_{I_c}/W_g depends on the ratio of two density-dependent quantities: the fracture energy G_{I_c}, calculated using weak layer density, and the gravitational potential energy W_g, determined by the overlying snow. Thus, low-density snow simultaneously reduces anticrack resistances within the storm-snow (G_{I_c}) and the gravitational driving force for propagation (W_g). These opposing effects partially cancel, keeping SI_{ANT} above unity across most of the snowpack even as SI_{sh} signals widespread shear failure.

Figure 1, introduced in Section 2.4, shows the combined stability matrix trajectory for this event. The storm begins in the "both stable" quadrant (upper right, open circle) before rapidly descending into the "shear unstable / anticrack stable", confirming that the January 13-15 event is characterized by shear-driven instability.

3.3 Avalanche data

The avalanche data panel displays timestamped observations from four independent sources; GeoPrevent (Meier et al., 2016), Snowbound Solutions (Johnson et al., 2018), the Utah Avalanche Center (UAC), and the Utah Department of Transportation (UDOT). Geoprevent technology, which emits radio waves and measures the reflected signal, has been operational along the Mount Superior and Hellgate avalanche slide paths in Little Cottonwood Canyon (LCC) for two full seasons. These slide paths are conveniently located ~1 km from the Atwater study plot, where DEID measurements are acquired. Snowbound Solution's infrasound system, which monitors low-frequency sound waves, has been deployed for several seasons along LCC and is currently used to inform avalanche-related safety decisions.

Additional user-submitted observations to the UAC, along with professional mitigation records supplied from UDOT will be used to cross-reference the avalanche detection systems to determine natural avalanches failing in new snow, along with providing additional snowpack stability context for each event. These datasets have not yet been formally analyzed to validate the combined stability matrix presented in this paper and are discussed more in Section 4.

4. SUMMARY AND FUTURE WORK

DENDRITE is still a work in progress tool that requires further testing and analysis in the upcoming season. It has the potential to be a physics-

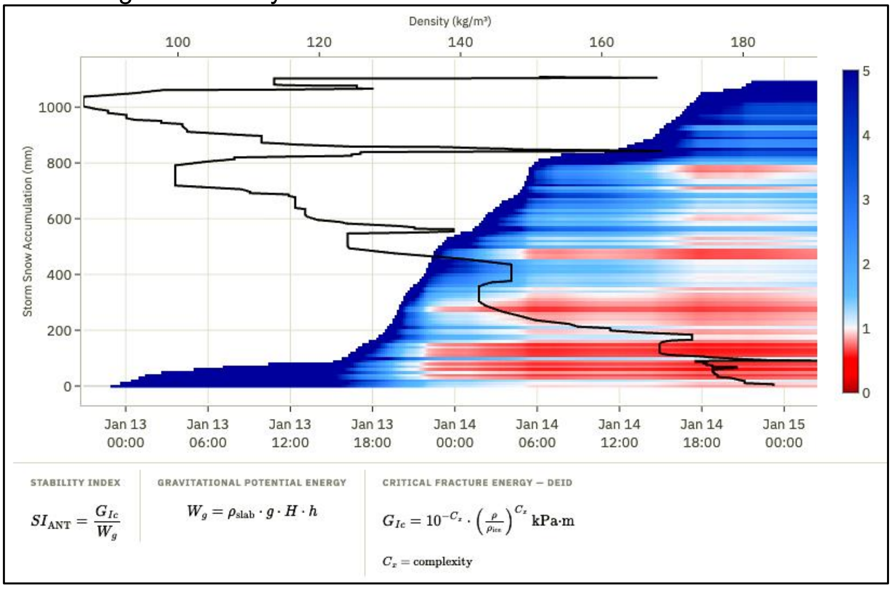

Figure 5. DEID-based anticrack stability index (SI_{ant}) heatmap for the January 13–15, 2024 storm. The y-axis is cumulative storm snow accumulation (mm); the x-axis is time (UTC). Blue: $SI_{ant} > 1$ (stable); red: $SI_{ant} > 1$ (unstable). Despite widespread shear instability, 65% of layer-time combinations remain anticrack-stable due to the compensating effect of low slab density on both fracture energy and gravitational potential energy.

based, real-time storm-snow avalanche decision-support tool that integrates DEID measurements of snowflake habit

and density with shear-based and anticrack-based stability models to produce a continuously updated, unified stability matrix. Each of these models can be run using DEID-measured parameters, or density-only best-fit formulations, enabling deployment with or without a DEID instrument. DENDRITE presents these stability outputs alongside real-time weather data and avalanche observations. Avalanche data aggregates records from Geoprevent, Snowbound Solutions, UAC, and UDOT, which allows practitioners to consult in parallel with the stability matrix during active storms.

Applied to the January 13-15, 2024 storm event in Little Cottonwood Canyon, a 53-hour, ~1100 mm event with low-density storm snow (56–167 kg m^{-3}), DENDRITE identifies widespread shear instability (SI_{sh} < 1 across 73% of tracked layer-time combinations) while the anticrack index remains predominantly stable (35% below 1). This contrast reflects the compensating effect of low-density storm-snow on both fracture energy and gravitational potential energy in the anticrack model. This is captured directly in the stability matrix trajectory, which spends most of the storm in the shear-unstable / anticrack-stable quadrant.

While the stability matrix qualitatively assesses snowpack structure, its accuracy cannot be validated without analysis of the avalanche observation datasets. These future studies will determine which detections were natural avalanches failing in new snow, and how well each of the two indices predicted for these failures. This will identify the relationship between SI_{Sh} and SI_{ANT}, and if one or the other is better for predicting storm-snow avalanches.

Furthermore, DENDRITE will be integrated with the High-Resolution Rapid Refresh (HRRR) numerical weather model to extend as a 48-hour forecast system. This extension, along with the validation of the storm-snow avalanche decision-support tool will be operationally focused, specifically designed to meet the needs of snow professionals.

COMPETEING INTERESTS

The DEID® and Particle Flux Analytics® are registered trademarks. The authors declare the following financial interests and/or personal relationships, which may be considered potential competing interests:

TJG is a scientific advisor for Particle Flux Analytics and holds an equity interest. TJG, DKS, and ERP are named patent holders for the DEID® (No. 11,674,878), which is licensed to

Particle Flux Analytics®. ERP and DKS have royalty interest in DEID® sales.

ACKNOWLEDGEMENTS

We thank Steven Clark of the Utah Department of Transportation (UDOT) for his continued support and direction throughout each winter season. We thank the entire Utah Avalanche Center (UAC) for their work in educating the public and encouraging collaboration across snow science disciplines. We thank Théo St. Pierre Ostrander of Geoprevent, and Scott Havens from Snowbound solutions for access to avalanche detection datasets. This material is based upon work primarily supported by the Innovations Deserving Exploratory Analysis (IDEA) grant, funded by the National Cooperative Highway Research Program through the National Academy of Sciences.

Lastly, we thank Allan Reaburn and Particle Flux Analytics, Inc. for their contributions to the development and advancement of the DEID. DEID development is also based upon work supported by the U.S. Department of Energy through SBIR Awards granted to Particle Flux Analytics, Inc. under contract numbers DE-SC0017168, DE-SC0022516, and DE-SC0025812. Particle Flux Analytics Inc. provided technical expertise. Particle Flux Analytics, Inc. owns invention licenses, proprietary data rights, and the copyrights and trademarks for the DEID.

REFERENCES

Adam, V., Bergfeld, B., Weißgraeber, P., van Herwijnen, A., and Rosendahl, P. L., 2024. Fracture toughness of mixed-mode anticracks in highly porous materials, Nat. Commun., 15, 7379, https://doi.org/10.1038/s41467-024-51491-7.

Bair, E. H., Simenhois, R., Birkeland, K., and Dozier, J., 2012. A field study on failure of storm snow slab avalanches, Cold Reg. Sci. Technol., 79–80, 20–28, https://doi.org/10.1016/j.coldregions.2012.02.007.

Chernov, R.A., 2024. Experimental determination of the coefficient of viscosity of dry snow, Ice and Snow, 64(2), 273-280, URL:https://journals.eco-vector.com/2076-6734/article/view/659281.

Conway, H. and Wilbour, C., 1999. Evolution of snow slope stability during storms, Cold Reg. Sci. Technol., 30, 67–77.

Eskeland, J. A. R., 2025. Real-time modeling of storm-snow anticrack instabilities using the Differential Emissivity Imaging Disdrometer (DEID), M.S. thesis, Department of Mechanical Engineering, University of Utah, Salt Lake City, UT, USA.

Hayes, P., Wilbour, C., Gibson, R., Marshall, H. P., and Conway, H., 2004. A simple model of snow slope stability during storms, in: Proceedings of the International Snow Science Workshop, 19–24 September 2004, 165–171.

Heierli, J. and Zaiser, M., 2006. An analytical model for fracture nucleation in collapsible stratifications, Geophys. Res. Lett., 33, L06501, https://doi.org/10.1029/2005GL025311.

Jamieson, J.B. and Johnston C. D, 2001. Evaluation of the shear frame test for weak snowpack layers, Annals of Glaciology,32:59–69, doi:10.3189/172756401781819472.

Johnson, J. B., Marshall, H. P., Loo, S. M., Nalli, B., Saurer, M., Havens, S., Colton, J., and Anderson, J. F., 2018. Detection and tracking of snow avalanches in Little Cottonwood Canyon, Utah using multiple small-aperture infrasound arrays, in: Proceedings of the International Snow Science Workshop, 7–12 October 2018, 616–620.

Kojima, K., 1967. Densification of Seasonal Snow Cover, Physics of Ice and Snow: Proc. Int. Conf. on Low Temperature Science, pages 929–952, Sapporo, Japan, Institute of Low Temperature Science. URL:https://api.semanticscholar.org/CorpusID:59030962

McClung, D. M., 2007. Fracture energy applicable to dry snow slab avalanche release, Geophys. Res. Lett., 34, L02503, https://doi.org/10.1029/2006GL028238.

Meier, L., Jacquemart, M., Blattmann, B., and Arnold, B., 2016. Real-time avalanche detection with long-range, wide-angle radars for road safety in Zermatt, Switzerland, in: Proceedings of the International Snow Science Workshop, 3–7 October 2016, 304–308.

Morrison, T. J., Meisenheimer, T., Garrett, T., Singh, D., Donovan, S., and Pardyjak, E., 2023. Relating storm-snow avalanche instabilities to data collected from the Differential Emissivity Imaging Disdrometer (DEID), Cold Reg. Sci. Technol., 210, 103839, https://doi.org/10.1016/j.coldregions.2023.103839.

Silberman, B. H., Morrison, T. J., Singh, D. K., Garrett, T. J., and Pardyjak, E. R., 2026. Optimizing the Gibson-Ashby model to predict the shear strength of storm-snow, unpublished manuscript.

Singh, D. K., Donovan, S., Pardyjak, E. R., and Garrett, T. J., 2021. A differential emissivity imaging technique for measuring hydrometeor mass and type, Atmos. Meas. Tech., 14, 6973–6990, https://doi.org/10.5194/amt-14-6973-2021.

Singh, D. K., Pardyjak, E. R., and Garrett, T. J., 2024. Time-resolved measurements of the densities of individual frozen hydrometeors and fresh snowfall, Atmos. Meas. Tech., 17, 4581–4598, https://doi.org/10.5194/amt-17-4581-2024.